Applications of photonic crystals in optical data storage

Tao Liu, Armis R. Zakharian, Radhakrishn Rathnakumar, Mahmoud Fallahi, Jerome V. Moloney, et al.

Tao Liu, Armis R. Zakharian, Radhakrishn Rathnakumar, Mahmoud Fallahi, Jerome V. Moloney, Masud Mansuripur, "Applications of photonic crystals in optical data storage," Proc. SPIE 5380, Optical Data Storage 2004, (9 September 2004); doi: 10.1117/12.556889

SPIE.

Event: Optical Data Storage Topical Meeting, 2004, Monterey, California, United States

Applications of photonic crystals in optical data storage

Tao Liu[+], Armis R. Zakharian[*], R. Rathnakumar[*], M. Fallahi[+],
J. V. Moloney [+,*], and M. Mansuripur[+]

[+]Optical Sciences Center and [*]Department of Mathematics, University of Arizona, Tucson, AZ 85721

ABSTRACT

We propose the general idea of constructing an ultra-compact optical pickup based on photonic crystals. A few of the optical components necessary for various functions of an optical head are designed and analyzed. These include a waveguide with a sharp bend, a directional coupler, a 3dB beam-splitter, a polarizing beam-splitter, and a Mach-Zehnder interferometer. The *Finite Difference Time Domain* (FDTD) method is used to simulate the suggested structures.

Key words: Integrated optical pickup; Micro-optical pickup; Photonic crystal pickup

I. Introduction

The optical pickup is one of the most important devices in an optical disk memory system. A pickup constructed from bulk or micro-optical elements requires complex and time-consuming fabrication, involving component assembly and alignment. By comparison, an integrated pickup that uses waveguides and integrated opto-electronics has many advantages [1,2]. One important improvement is a significant reduction in size compared to pickups constructed of bulk optics. However, devices built with conventional integrated optical techniques are still on the order of millimeters in their linear dimensions. Large-scale integration of such devices (for example, in applications that involve parallel read/write operations) requires further miniaturization. With the advent of a new optical material, the photonic crystal, this goal seems to be within reach.

The basic idea of photonic crystals was initially proposed in 1987 [3]. In the intervening years, superior properties of photonic crystals attracted increasing attention from researchers around the world. Photonic crystals consist of a periodic arrangement of dielectric or metallic nanostructures, exhibiting a photonic bandgap that prohibits the propagation of light in one, two, or three dimensions over a finite spectral range. With this property, light can be controlled at the length-scale of an optical wavelength, and many traditional as well as novel optical components may be constructed. Photonic crystal devices are usually much smaller than their conventional counterparts; therefore, an optical pickup constructed from photonic crystals is expected to have an appreciable size advantage over those previously proposed.

Before building a functional pickup, one must demonstrate individual components with the necessary functionalities. These components can then be interfaced with each other and combined to form an integrated device. We will introduce the general idea of a compact optical head based on photonic bandgap crystals, then present specific designs and simulation results for several components that we believe are needed in a fully-integrated optical pickup. The simulations are done with a *Finite Difference Time Domain* (FDTD) [4] computer code.

II. Design of optical components with photonic crystals

Figure 1(a) shows a simple prototype for a compact optical pickup. This device uses a square-lattice photonic crystal consisting of dielectric columns in air. Certain rows and columns have been removed from this otherwise perfect crystal to form guiding channels. The pitch of the crystal, *a*, which depends on the operating wavelength, is usually less than one half of one wavelength. The diameter of the dielectric columns is chosen such that a large photonic bandgap exists around the operating wavelength. In this setup, a laser diode can be attached to the device in order to couple light into the waveguide. The input light goes through the first sharp (~90°) bend and reaches the optical disk located in the near-field of the outlet. The light reflected from the disk is coupled back into the waveguide and, with the help of a directional coupler and another sharp bend, nearly half of this reflected light will reach the detector. (An absorber

Optical Data Storage 2004, edited by B. V. K. Vijaya Kumar, Hiromichi Kobori,
Proceedings of SPIE Vol. 5380 (SPIE, Bellingham, WA, 2004)
0277-786X/04/$15 · doi: 10.1117/12.556889

should be used to remove the fraction of the input light that does not make it to the optical disk, thus preventing spurious reflections.) Since this proposed device is designed to work in the near field, no focusing scheme is required. Needless to say, the same functionality could be implemented with conventional optical waveguides; however, one advantage of photonic crystals is that the final device ends up being much smaller. This will be illustrated with the designs of various optical components in the following sections.

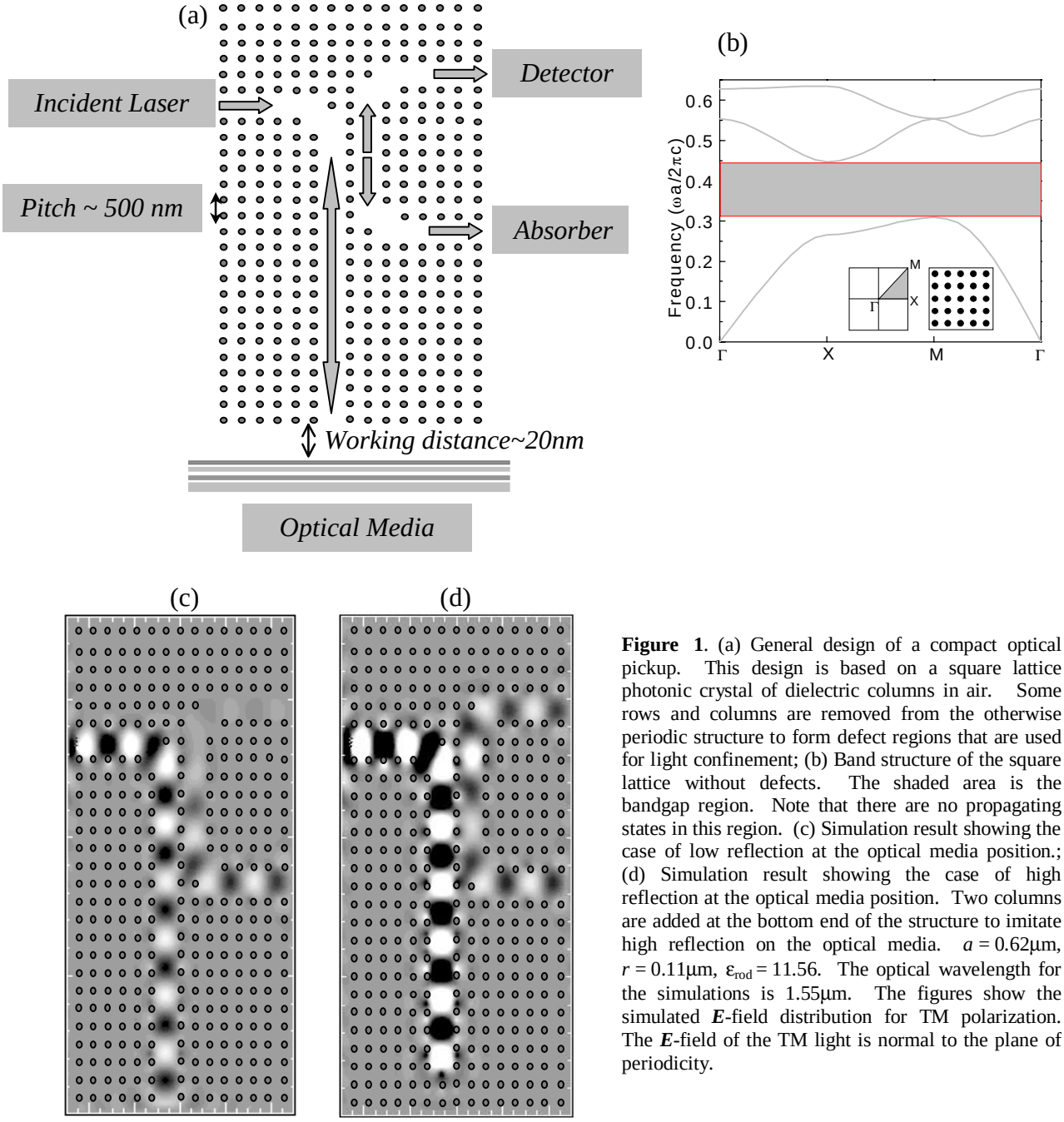

Figure 1. (a) General design of a compact optical pickup. This design is based on a square lattice photonic crystal of dielectric columns in air. Some rows and columns are removed from the otherwise periodic structure to form defect regions that are used for light confinement; (b) Band structure of the square lattice without defects. The shaded area is the bandgap region. Note that there are no propagating states in this region. (c) Simulation result showing the case of low reflection at the optical media position.; (d) Simulation result showing the case of high reflection at the optical media position. Two columns are added at the bottom end of the structure to imitate high reflection on the optical media. $a = 0.62\mu m$, $r = 0.11\mu m$, $\varepsilon_{rod} = 11.56$. The optical wavelength for the simulations is 1.55μm. The figures show the simulated ***E***-field distribution for TM polarization. The ***E***-field of the TM light is normal to the plane of periodicity.

For optical storage applications, the light has to be confined in all three dimensions. In the structure shown in Figure 1(a), light is confined in the plane of periodicity by the bandgap effect. In the direction normal to this plane, light can

be confined by two other mechanisms. The first is to use two omni-directional reflectors [5] to sandwich the photonic crystal. The second is to make photonic crystals of air holes in a dielectric medium, instead of dielectric columns in air. For this kind of structure, defect regions have higher refractive index than the air claddings (or some other low-index claddings) and therefore the light can be confined by total internal reflection (TIR) in the vertical direction. In this paper, we choose photonic crystals of dielectric columns in air for the simplicity of simulations. Unless stated, otherwise all the simulated structures in this paper have the following parameters: the pitch of the square lattice is 0.62μm, the radius of the columns is 0.11μm, and the dielectric constant of the columns is 11.56. The optical wavelength in the simulations is 1.55μm. (This wavelength is used in telecommunication area and enables the designs to choose from a wide class of high-index materials, such as Si and GaAs. For optical data storage applications, however, it is preferred to use shorter wavelengths in the blue regime of the spectrum.) For the selected parameters, the photonic crystal has a large bandgap centered around 1.55μm for TM polarized light. The band structure [6] for a perfect photonic crystal with the above parameters is shown in Figure 1(b) and the bandgap region is shown as a shaded area. The horizontal axis is the wave vector, while the vertical axis represents the frequency. Note that the frequencies are normalized by the period of the photonic crystal and the speed of light in free space. If the incident light falls inside this bandgap region, it is forbidden to propagate inside the structure. By introducing various defects, we obtain defect states in the bandgap, which states form the basis for the functional devices described in the following sections.

Two simulation results are given in Figures 1(c) and (d) in order to illustrate the working principle of the proposed optical pickup described in Figure 1(a). For crystal structure in Figure 1(c), the incident light has small reflection at the bottom facet. Therefore only a small fraction of light will go back into the structure and reaches the detector. This case imitates low reflection from the optical disc. For crystal structure shown in Figure 1(d), however, two extra dielectric columns are added at the bottom output facet and this causes high reflection when the incident light arrives. As a result, most of the light will go back into the structure and reaches the detector with the help of the directional coupler. This case imitates high reflection from the optical disc. The ***E***-field distributions are shown in Figures 1(c) and (d). It can be clearly seen that the two cases with low and high reflection on the optical disc yield very different results at the detector: the signal received by the detector in the high reflection case is around 25 times stronger than that for the low reflection case.

The design shown in Figure 1(a) is composed of individual optical components that include: optical waveguide, waveguide sharp bend and directional coupler. These components will be explained in detail below, together with some other components that are useful for parallel read/write operations such as beam splitter, Mach-Zehnder interferometer, and polarizing beam-splitter. All the simulations presented in this paper are done in the infrared regime. The photonic crystals in the infrared regime have relatively larger feature size compared to their visible-light counterparts, which makes fabrication and characterization easier. The same effects can be readily extended to the visible regime.

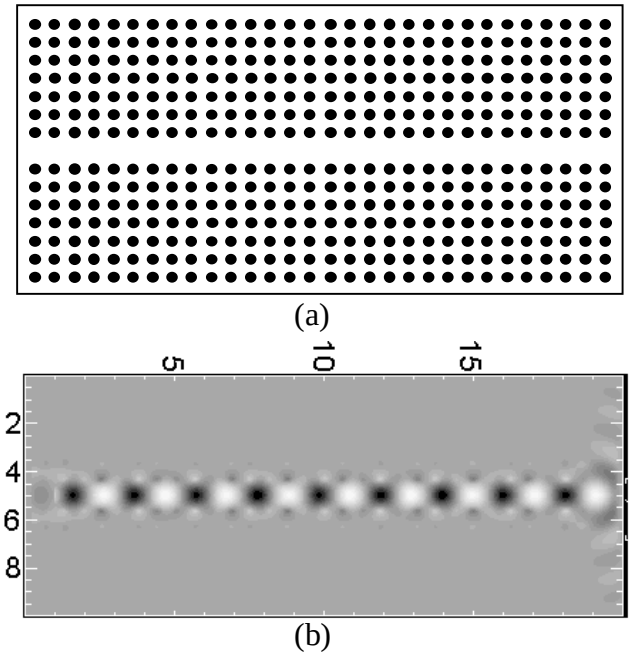

Figure 2. (a) Diagram of a photonic crystal waveguide based on a square lattice of dielectric columns in air. The waveguide is formed by removing one row of the dielectric columns: $a = 0.62\mu m$, $r = 0.11\mu m$, $\varepsilon_{rod} = 11.56$. Unit: μm. (b) Simulated *E*-field distribution when light is coupled into the waveguide from the left end. The optical wavelength is 1.55μm.

1. Optical waveguide

Waveguides are indispensable components of integrated optical devices. In conventional waveguides, light is guided by TIR. Since TIR happens when light is incident from a high-index to a low-index medium, conventional guiding can be achieved only within the high-index medium. In photonic crystal devices, however, light is guided through a novel mechanism, the photonic bandgap, and may therefore be confined in a low-index medium at the length-scale of one optical wavelength.

Figure 2(a) shows a square-lattice photonic crystal of dielectric columns in air with an air-channel comprising the guiding region. This air-channel is formed by removing one row of the dielectric columns. This waveguide structure can also be viewed as an air-channel surrounded by two perfect photonic crystal reflectors. Due to the introduction of this line defect, light can be confined. The ***E***-field distribution for TM light propagation is shown in Figure 2(b). It can be seen that light is tightly confined in the defect region. By increasing the width of the air-channel (the distance between the two photonic crystal reflectors), we can also get multimode operation. This is similar to the conventional optical waveguide and is the basis for our beam splitter design described below.

2. Waveguide bend

Waveguide bends are the basis for constructing large-scale integrated optical circuits. One weakness of conventional waveguides with TIR guiding is the difficulty of creating sharp bends. Unless the radius of the bend is large (compared to the wavelength), much of the light will escape the sharp bend. This is a serious problem in creating dense integrated circuits, since the space required for large-radius bends is at a premium. It is also one of the main reasons why we prefer photonic crystals over conventional waveguides. If a sharp bend is created in a photonic crystal guide, it is impossible for light to escape; the only problem is posed by back-reflections at the sharp corner. Fortunately, it turns out that nearly 100% transmission is possible to obtain in such waveguides [7]. Figure 3 shows a 90° bend in a square-lattice photonic crystal waveguide that consists of dielectric columns in air; the ***E***-field distribution for TM light propagation is shown on the right-hand side. The transmission efficiency of this waveguide is ~ 90%.

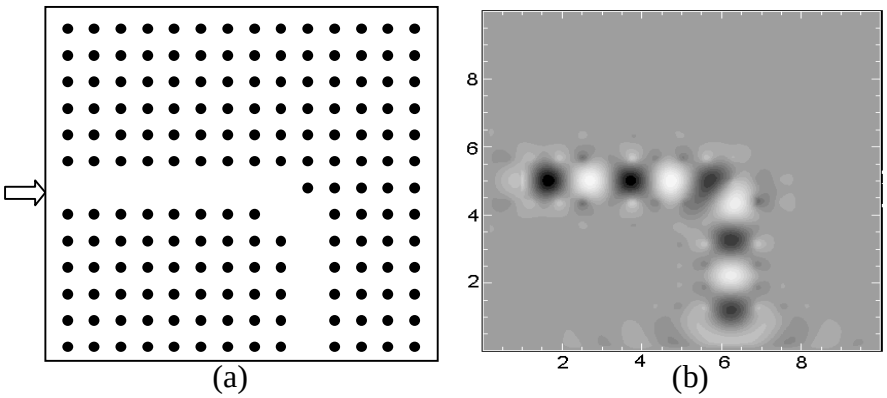

Figure 3. (a) Diagram of a sharp bend in a square lattice photonic crystal of dielectric columns in air. The bend is formed by removing some dielectric columns. $a = 0.62\mu m$, $r = 0.11\mu m$, $\varepsilon_{rod} = 11.56$. Unit: μm. (b) Simulated *E*-field distribution when light is coupled into the guide from the left end. The optical wavelength is 1.55μm.

3. Directional Coupler

A directional coupler is the basis for the compact design of an optical pickup device shown in Figure 1(a). It is also extensively used in conventional integrated optics for power splitting, wavelength routing, etc. A directional coupler is composed of two identical waveguides that are close to each other. Due to evanescent coupling between the waveguides, the light entering one waveguide will transfer back and forth between the two. One interesting feature of a photonic crystal-based directional coupler is its

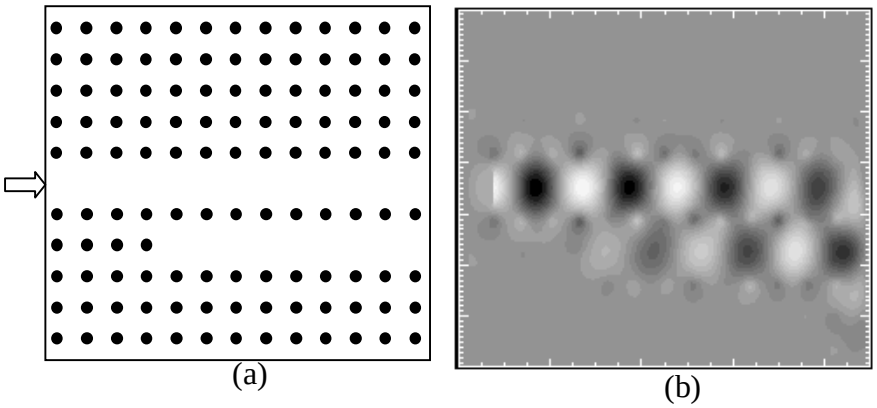

Figure 4. (a) Diagram of a directional coupler in a square lattice photonic crystal of dielectric columns in air. The directional coupler is formed by removing two rows of columns. $a = 0.62\mu m$, $r = 0.11\mu m$, $\varepsilon_{rod} = 11.56$. (b) Simulated ***E***-field distribution when light is coupled into the directional coupler from the left end. The optical wavelength is 1.55μm.

extremely small size compared to its conventional counterpart. For the directional coupler shown in Figure 4(a), the length of the coupling region is only ~ 6μm. From the simulation result shown in Figure 4(b), it can be seen that equal power splitting is obtained at the end of this directional coupler. This is another reason why photonic crystal-based optical pickups have the advantage of reduced size.

4. Beam splitter

Another important component that will be useful for parallel readout in an integrated optical pickup is a beam-splitter. In Figure 5(a), we propose a 3 dB photonic crystal beam-splitter based on the multi-mode interference (MMI) effect in a multi-mode waveguide [8]. The length of the device in Figure 5(a) is seen to be fairly long because partial reflection from the input and output facets must be avoided in order to determine the power splitting efficiency accurately in the FDTD simulation. By using a pulse excitation in the simulation and a structure with very long input and output single mode waveguides, as shown in Figure 5(a), we are able to separate the input pulse from the reflected pulses. By Fourier transforming these pulses, we can calculate the splitting efficiency accurately. Of course, the size of a real device is primarily dependent on the length of the multimode section. In Figure 5(a), the multimode section is only around 4μm long. With this splitter, the coupling efficiency from the input waveguide into each output channel is found to be ~ 45%. The remaining 10% of the light is lost due to imperfect coupling between the input (single-mode) waveguide and the intermediate (multi-mode) section. The splitter's operating bandwidth is greater than 100 nm. Compared to a conventional MMI beam-splitter, device size is substantially reduced and the operating bandwidth is greatly enhanced.

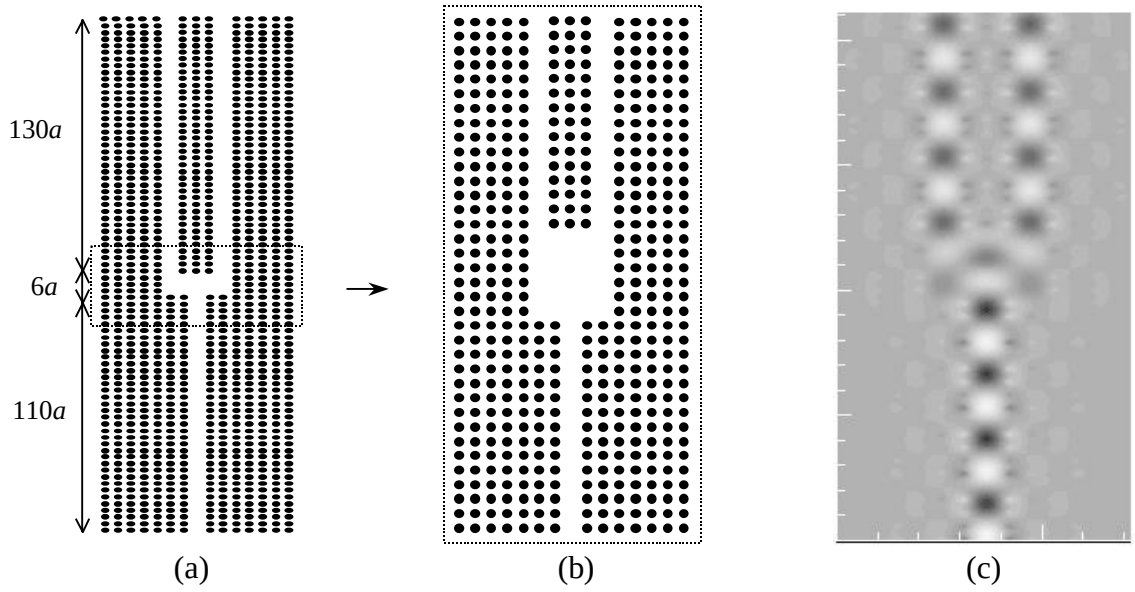

Figure 5. (a) Diagram of a waveguide beam splitter in a square lattice photonic crystal of dielectric columns in air. $a = 0.62\mu m$, $r = 0.11\mu m$, $\varepsilon_{rod} = 11.56$. (b) Magnified view of the region around the multimode waveguide section. (c) Simulated ***E***-field distribution when light is coupled into the directional coupler from the bottom end. The optical wavelength is 1.55μm.

5. Polarizing beam-splitter

A polarizing beam-splitter (PBS) may be used to separate an input light beam into its linear polarization constituents. In bulk optics a multilayer coating with different responses to TM / TE light is often used for this purpose. In conventional optical pickup, a PBS is often used to re-direct the signal light that is reflected from the optical disc to the detectors. In Figure 6(a) we propose a PBS built from a triangular photonic crystal of air holes in a dielectric material. This structure has a bandgap for TE light only, so TE light can be guided through the photonic bandgap effect. Since the guiding region has a higher effective index than the surrounding areas, TM light can also be guided through index contrast [9]. Due to the special dispersion properties of this device, the two waveguides are de-coupled for TE light [10] and

therefore TE light will remain confined in the direct channel. For TM light, however, the situation is completely different. The coupling strength of the two waveguides for TM light is much stronger than that for TE light. As a result, TM light will transfer fully from the direct channel into the adjacent channel.

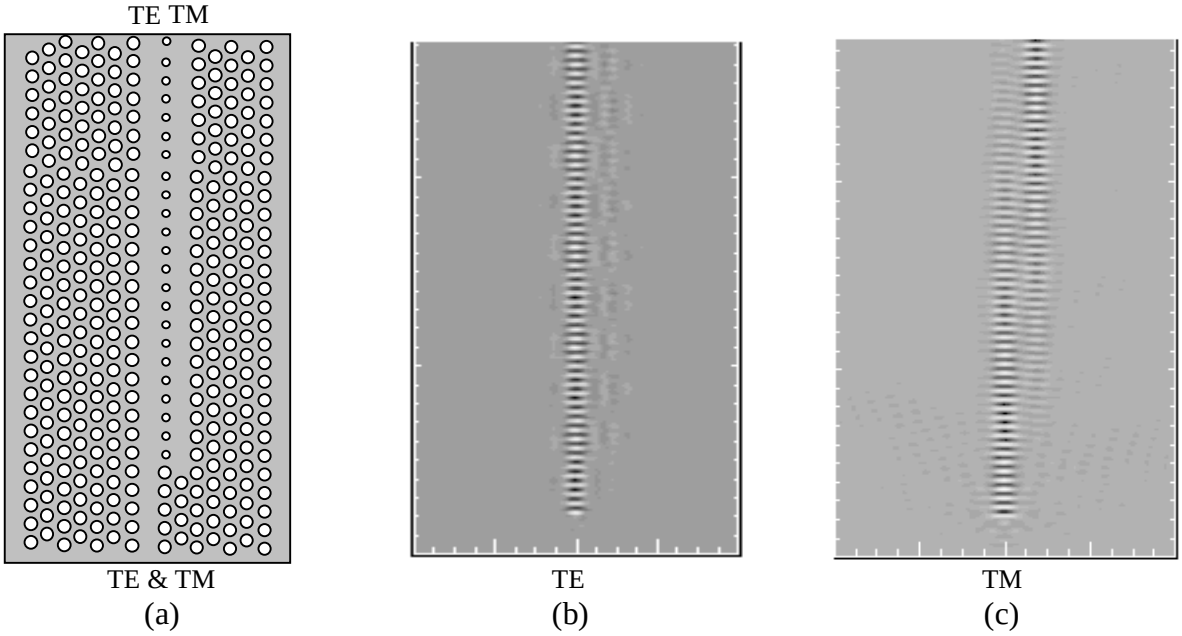

Figure 6. (a) Diagram of the proposed PBS; a = 0.45μm, r = 0.16μm, r_{def} = 0.10μm, $\varepsilon_{\text{dielectric}}$ = 11.56. (b) Simulated ***H***-field distribution. The ***H***-field of the TE light is normal to the plane of periodicity. (c) Simulated ***E***-field distribution. The ***E***-field of the TM light is normal to the plane of periodicity. Light is coupled into the PBS from the bottom end. The optical wavelength is 1.55μm.

In Figure 6, the required length of the directional coupler for separating TM and TE is only around 25μm. The radius of the air holes in between the two waveguides is 0.10μm, instead of 0.16μm for the normal air holes. The ***H***-field component for TE light propagation is shown in Figure 6(b), while the ***E***-field component for TM light is shown in Figure 6(c). It can be seen that most TE light remains in the direct channel and that TM light almost totally transfers into the adjacent channel. FDTD simulations are used to calculate the efficiency of the PBS. The extinction ratios are 16dB for TE light and 21dB for TM light. A photonic crystal sharp bend can be added to the end of this PBS to further separate the two polarizations.

6. Mach-Zehnder interferometer

Converting a cw laser beam into a signal that can be recorded on an optical disk requires optical modulators, especially when the same laser is used to write several tracks in parallel. External optical modulators are usually built using interferometers that are controlled with an electro-optical effect. Figure 7 shows a Mach-Zehnder interferometer constructed with a cascade of two MMI beam-splitters. When the two arms are identical as in Figure 7(a), the beams emerging from the two arms are added constructively at the output waveguide and therefore high transmission ~90% is achieved at the output. In Figure 7(b), five extra columns are added in the middle section of the right arm; the distance between two extra columns is twice the crystal period. These five extra columns form a coupled resonator optical waveguide (CROW) [11]. The light propagates at different velocity in the CROW compared to the normal linear waveguide. The size of the extra columns and the length of the CROW are chosen such that a 180° phase shift is introduced between the two arms. As a result, the two beams emerging from the arms are added destructively at the output waveguide and, therefore, transmitted light is barely noticeable in Figure 7(b). In Figure 7(c), five extra columns with the same parameters are also added to the left arm. Therefore the two arms are in phase again and we obtain high transmission. The computed ***E***-field distributions in the above three cases for TM light are shown in Figures 7(a), (b),

and (c). If the arms of this interferometer are filled with an actively controllable material (e.g., electro-optic material), the device can be used as an active, photonic_crystal-based modulator.

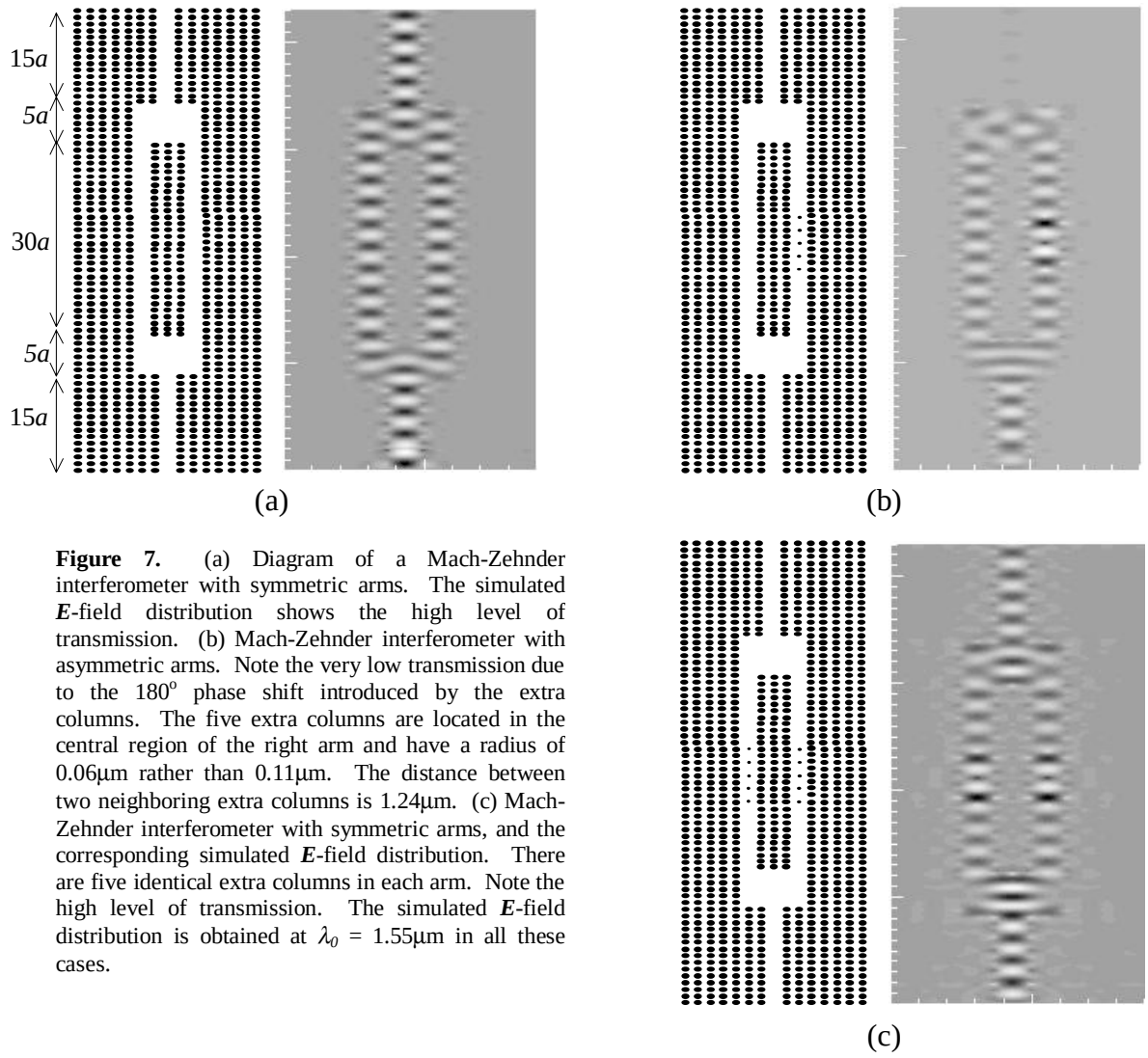

Figure 7. (a) Diagram of a Mach-Zehnder interferometer with symmetric arms. The simulated ***E***-field distribution shows the high level of transmission. (b) Mach-Zehnder interferometer with asymmetric arms. Note the very low transmission due to the 180^o phase shift introduced by the extra columns. The five extra columns are located in the central region of the right arm and have a radius of 0.06μm rather than 0.11μm. The distance between two neighboring extra columns is 1.24μm. (c) Mach-Zehnder interferometer with symmetric arms, and the corresponding simulated ***E***-field distribution. There are five identical extra columns in each arm. Note the high level of transmission. The simulated ***E***-field distribution is obtained at λ_0 = 1.55μm in all these cases.

III. Fabrication of photonic crystal optical components

We use Electron-beam lithography (EBL) for the fabrication of photonic crystal devices. The fabrication procedures are schematically illustrated in Figure 8. The wafers are either silicon-on-insulator (SOI) or GaAs. A layer of SiO_2 deposited on top of the wafer acts as an intermediate etching mask for pattern transfer. E-beam resist PMMA is spun on SiO_2. During E-beam writing, pre-defined patterns are written into PMMA. The exposed resist is removed during development in MIBK:IPA solution and the patterns are in PMMA at this moment, as illustrated in Figure 8(2). The patterns are first transferred from PMMA to SiO_2 with ECR-RIE etching and the mixture of CF_4 and H_2 gases is used for this step. For pattern transfer from SiO_2 to the wafer, a mixture of CF_4 and O_2 gases is used for SOI and a mixture of CH_4 and Cl_2 gases for GaAs. Finally, the residual SiO_2 intermediate etching mask is removed by dipping the wafer in HF solution. Some simple optical components, including straight waveguide, directional coupler, etc., are shown in Figure 9. We will report the results of measurement and characterization of these devices in a separate publication.

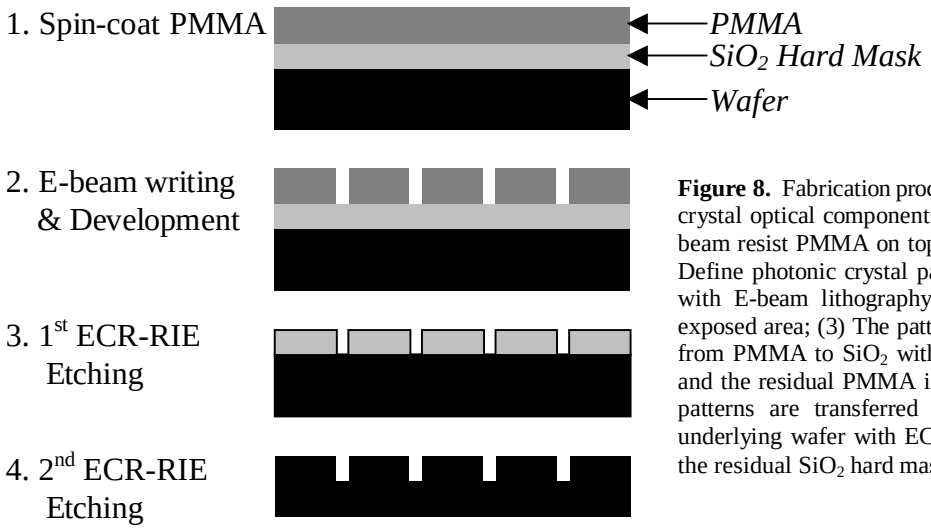

Figure 8. Fabrication procedures of photonic crystal optical components: (1) Spin-coat E-beam resist PMMA on top of the sample; (2) Define photonic crystal patterns into PMMA with E-beam lithography, then remove the exposed area; (3) The patterns are transferred from PMMA to SiO_2 with ECR-RIE etching and the residual PMMA is removed; (4) The patterns are transferred from SiO_2 to the underlying wafer with ECR-RIE etching and the residual SiO_2 hard mask is removed.

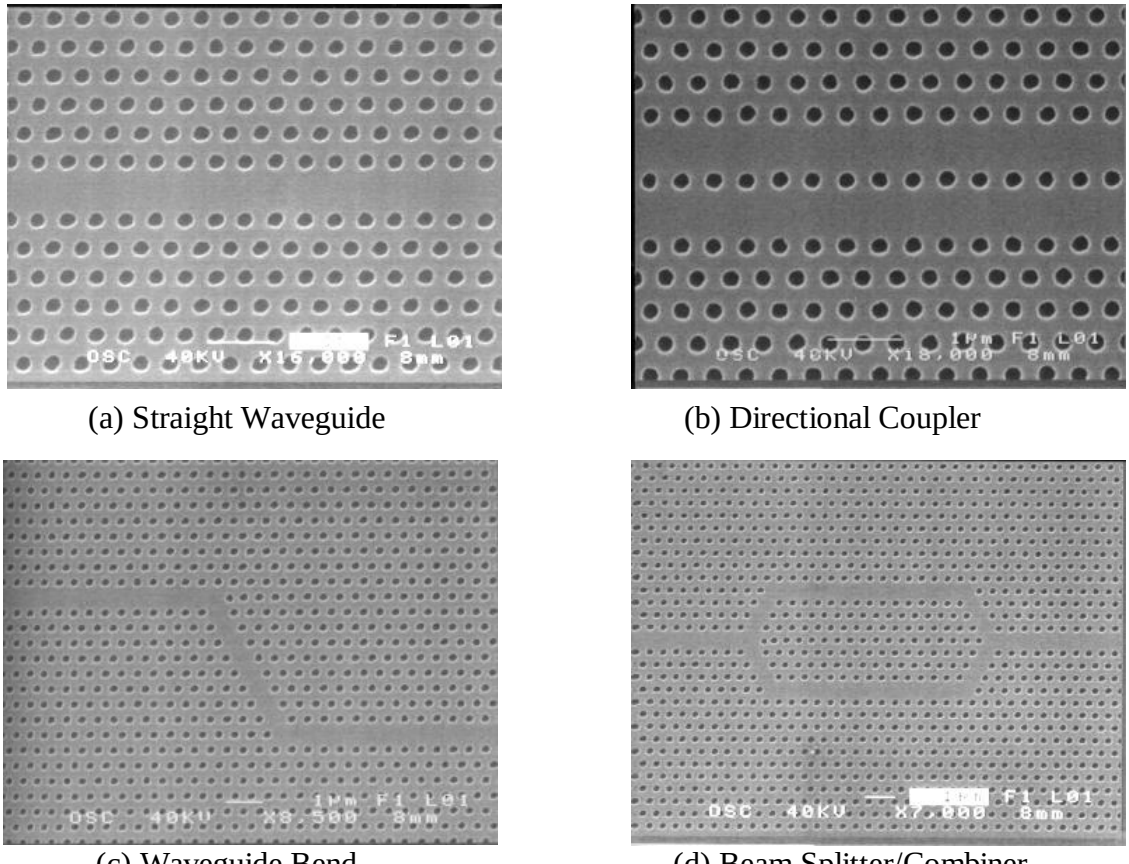

(a) Straight Waveguide

(b) Directional Coupler

(c) Waveguide Bend

(d) Beam Splitter/Combiner

Figure 9. Scanning Electron Micrographs (SEM) of several optical components that have been fabricated: (a) straight waveguide; (b) directional coupler with one row of air holes in between adjacent channels; (c) Two 120° sharp bends defined in a triangular photonic crystal; (d) beam splitter/combiner based on Y-junctions in a triangular photonic crystal. For all the patterns, the period is 500nm and the hole diameter is 250nm. The wafer is SOI.

IV. Conclusion

We presented the idea of constructing an ultra-compact optical pickup using photonic bandgap crystals. Some essential optical components were designed and simulated with the FDTD method. Aside from novel functional characteristics, these components have one common advantage over their conventional counterparts: dramatic size reduction. This property, which enables the construction of ultra-compact pickups, is also promising in the context of very large-scale optical integration. Some preliminary fabrication results with E-beam lithography were also presented.

REFERENCES

1. S. Ura, T. Suhara, and H. Nishihara, "An integrated-optic disk pickup device," *J. Lightwave Technol.*, vol. LT-4, no. 7, pp. 913-917, Jul. 1986.
2. T. Shiono, and H. Ogawa, "Planar-optic-disk pickup with diffractive micro-optics," *Appl. Opt.*, vol. 33, no. 31, pp. 7350-7355, Nov. 1994.
3. E. Yablonovitch, "Inhibited spontaneous emission in solid-state physics and electronics," *Phys. Rev. Lett.*, vol. 58, no. 20, pp. 2059-2062, May 1987.
4. A. Taflove, Computational Electromagnetics: The Finite-Difference Time-Domain Method. Artech, Boston, Mass., 1995.
5. Y. Fink, J. N. Winn, S. Fan, C. Chen, J. M, J. D. Joannopoulos, and E. L. Thomas, "A dielectric omnidirectional reflector," *Science*, vol. 282, pp. 1679-1682, Nov. 1998.
6. S. G. Johnson, and J. D. Joannopoulos, "Block-iterative frequency-domain methods for Maxwell's equations in a plane wave basis," *Opt. Express*, vol. 8, pp. 173-190, Jan. 2001.
7. A. Mekis, J. C. Chen, I. Kurland, S. Fan, P. R. Villeneuve, and J. D. Joannopoulos, "High transmission through sharp bends in photonic crystal waveguides," *Phys. Rev. Lett.*, vol. 77, pp. 3787-3790, Oct. 1996.
8. L. B. Soldano and E. C. M. Pennings, "Optical multi-mode interference devices based on self-imaging: Principles and applications," *J. Lightwave Technol.*, vol. 13, pp. 615-627, Apr. 1995.
9. P. I. Borel, L. H. Frandsen, M. Thorhauge, A. Harpoth, Y. X. Zhuang, M. Kristensen, and H. M. H. Chong, "Efficient propagation of TM polarized light in photonic crystal components exhibiting band gaps for TE polarized light," *Opt. Express*, vol. 11, no. 15, pp. 1757-1762, Jul. 2003.
10. S. Boscolo, M. Midrio, and C. G. Someda, "Coupling and decoupling of electromagnetic waves in parallel 2D photonic crystal waveguides," *IEEE J. Quantum Electron.*, vol.38, pp. 47-53, Jan. 2002.
11. N. Stefanou, and A. Modinos, "Impurity bands in photonic insulators," *Phys. Rev. B*, vol. 57, no. 19, pp. 12,127-12,133, May 1998.